ACS APPLIED MATERIALS & INTERFACES

www.acsami.org
Research Article

Self-Assembly of Microstructured Protein Coatings with Programmable Functionality for Fluorescent Biosensors

Suna Jo, Erin Pearson, Donghoon Yoon, Jungkwun Kim, and Won Min Park*

Cite This: ACS Appl. Mater. Interfaces 2024, 16, 63284−63294
Read Online

ABSTRACT: Proteins, as genetically programmable functional macromolecules, hold immense potential as biocompatible self-assembling building blocks, owing to their versatility in building coating materials and programming their functionality genetically. In this study, we demonstrate a modular self-assembly of protein coatings that are genetically programmable for a biosensor application. We designed and produced recombinant fusion protein building blocks to form microstructured coatings on diverse substrates, such as glass or polymers, through thermally triggered liquid−liquid phase separation and an orthogonal high-affinity coiled-coil interaction. We incorporated fluorescence proteins into coatings and controlled the protein density to enable fluorescence imaging and quantification in a low-resource setting. Then, we created a coating for a calcium biosensor using a genetically engineered calcium indicator protein. This protein coating served as the foundation for our smartphone-based fluorescent biosensor, which successfully measured free calcium concentrations in the millimolar range at which extracellular calcium homeostasis is maintained. Using this fluorescent biosensor, we were able to detect abnormal physiological conditions, such as mild or moderate hypercalcemia. We envision that this modular and genetically programmable functional protein coating platform could be extended to the development of highly accessible, low-cost fluorescent biosensors for a variety of targets.

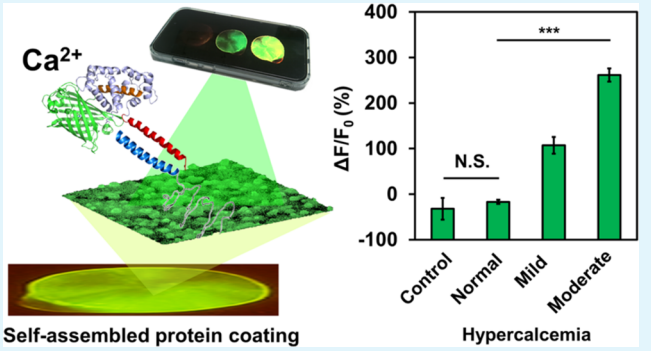

KEYWORDS: *protein coating, biosensors, calcium indicators, hypercalcemia, self-assembly, protein engineering, coiled coils, elastin-like polypeptide*

1. INTRODUCTION

Proteins have been exploited to build coating materials for a variety of applications in food packaging,[1,2] drug delivery,[3−6] tissue engineering,[7−9] biosensors,[10−13] biological adhesives,[14] and regenerative medicine.[3] Protein coatings offer a promising approach for creating functional surfaces with tailored properties such as antifouling activity,[15−18] selective binding affinity,[19] controlled release of therapeutics,[20,21] controlled interactions of nanoparticles with cell membrane,[5,6] and modulation of energy transfer for biosensing.[13] Such functional coatings include amyloid-based genetically modified protein coatings created via self-assembly, whose functionalities were programmed for biotemplating,[22] biocatalysis,[23] and bacterial sensors.[10] Recombinant curli nanofibers were engineered to create biofilms with biocatalytic functions, where the curli nanofibers enabled modular and site-specific enzyme immobilization.[24,25]

In coating fabrication, microstructure formation has a significant impact on the functionality and performance. Mechanical or physical properties of protein coating materials have been modulated through the control of microstructures,[10,26−28] which are influenced by the conformation, binding interaction, and topology of protein building blocks. An example is thin solid films of protein-block copolymer conjugates in which microphase-separated structures yielded high protein loading and biocatalytic activity.[29] Another example includes a superhydrophobic coating with microstructures, which were manipulated by the phase transition of lysozyme.[28] This coating presented excellent mechanical and thermal stability and the capability to drive protein crystallization.

Recombinant proteins have been used as versatile building blocks that present excellent programmability to self-assemble biomaterials, including coating materials.[29,30] Multiple genes can be recombined genetically and modularly to introduce self-assembling properties as well as a variety of functionalities, followed by protein expression and purification using well-

Received: August 22, 2024
Revised: October 16, 2024
Accepted: October 29, 2024
Published: November 6, 2024

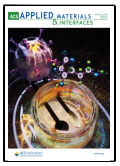

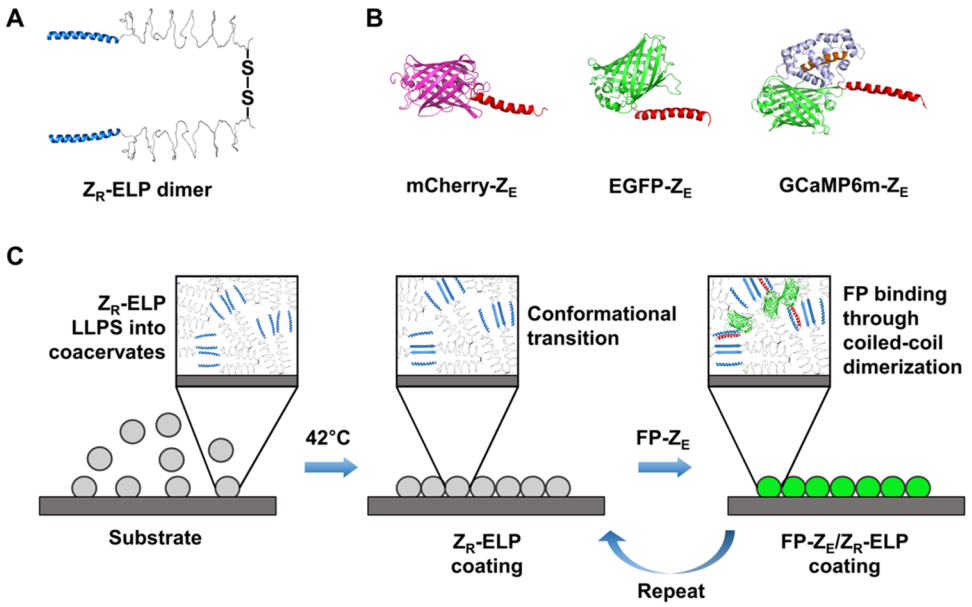

Figure 1. Schematic illustration of the self-assembly of a microstructured protein coating. (A) Dimeric topology of Z_R-ELP formed through a disulfide bond. (B) Three recombinant fluorescent proteins fused with a coiled-coil tag (FP-Z_E): mCherry-Z_E, EGFP-Z_E, and GCaMP6m-Z_E. (C) Coating self-assembly process: The microstructures are initially formed through liquid−liquid phase separation (LLPS) of the Z_R-ELP protein. These coacervates from LLPS adhere to surfaces and become interconnected. The structural changes associated with the transition of coiled-coil α-helices (Z_R) to β-sheets at 42 °C stabilize the microstructures of the coating. Upon incubation, FP-Z_E binds to the Z_R domains within the microstructures through strong coiled-coil dimerization of Z_E and Z_R, resulting in fluorescent protein coatings. This process is repeated to control the density of proteins within a coating.

established protocols.[30] Despite their genetic programmability, processing protein materials is often required through chemical modifications using organic solvents[31−33] or chemical reagents for covalent substrate attachment, cross-liking, or conjugation with block copolymers.[29,33] These additional steps along with additional washing or functionalization in protein coating fabrication present challenges in manufacturing process development and may limit functionality due to the potential protein denaturation. Moreover, production of recombinant curli nanofibers is challenging, particularly when multiple functional domains need to be introduced.[24,25] Thus, a system of recombinant protein coating assembly under biocompatible conditions would be desirable for the development of highly functional coating materials.

In this study, we demonstrate the self-assembly of modular, biocompatible protein coatings with genetic programming of functions and properties. We exploited two distinct protein motifs, an elastin-like polypeptide (ELP) and high-affinity coiled coils, to achieve coating assembly on a variety of substrate materials, manipulate microstructured morphology for a high surface area, and incorporate globular functional domains to protein coatings. ELPs are tropoelastin-derived biomimetic peptides that undergo thermally triggered liquid−liquid phase separation. The inverse phase transition results in the formation of insoluble coacervates from soluble proteins in an aqueous solution.[34] Coiled coils are the α-helices that bind to each other to form a superhelical bundle. Because of their exceptional binding affinity and specificity, coiled coils have been used to program protein assemblies in various systems.[35−37] We recombined ELP, coiled coils, and functional protein modules into fusion protein building blocks that form a coating material through a simple, chemical-free, and water-based process under biocompatible conditions (Figure 1).

We used this coating platform to fabricate a smartphone-based biosensor device for the detection of hypercalcemia. Current calcium biosensors include photonic polymers and[38,39] functionalized nanoparticles,[40,41] which provide millimolar resolution, as well as chemical fluorescence indicators[42−44] and microelectrodes.[45] While chemical fluorescent indicators like fura-2[42] and rhod-5N[43] are widely used to quantify Ca^{2+} in micromolar concentrations, they often experience nonspecific binding and interference from other cations such as Na^+, K^+, and Mg^{2+}. Microelectrodes, although capable of a wide dynamic range and stable voltage readings with a subnanomolar resolution,[45] are limited by their slow response to calcium changes and susceptibility to fouling, which may hinder real-time monitoring.[46,47] To address these limitations, we exploited a genetically encoded fluorescent calcium ion indicator, GCaMP, which provides high specificity for calcium ions and rapid response times.[48] We integrated GCaMP into a protein coating such that the coating exhibits fluorescence dependent on the concentration of Ca^{2+}. Employing a light-emitting diode (LED) transilluminator and smartphone camera, we measured the fluorescence from the protein coating and quantified the Ca^{2+} concentrations in biological fluids (0.5−3 mM) that are relevant to mild and moderate hypercalcemia. This approach offers a simple and low-cost solution suitable for resource-limited settings.

2. RESULTS AND DISCUSSION

2.1. Self-Assembly of a Microstructured Functional Coating Using Recombinant Proteins. We exploited two distinct types of protein−protein interactions to self-assemble microstructured coating materials and genetically program functionality. A pair of heterodimeric coiled-coil proteins (Z_E:Z_R, colon denotes heterodimerization) with a high-affinity binding interaction (dissociation constants $K_D \sim 10^{-15}$ M)[49,50]

https://doi.org/10.1021/acsami.4c14249
ACS Appl. Mater. Interfaces 2024, 16, 63284−63294

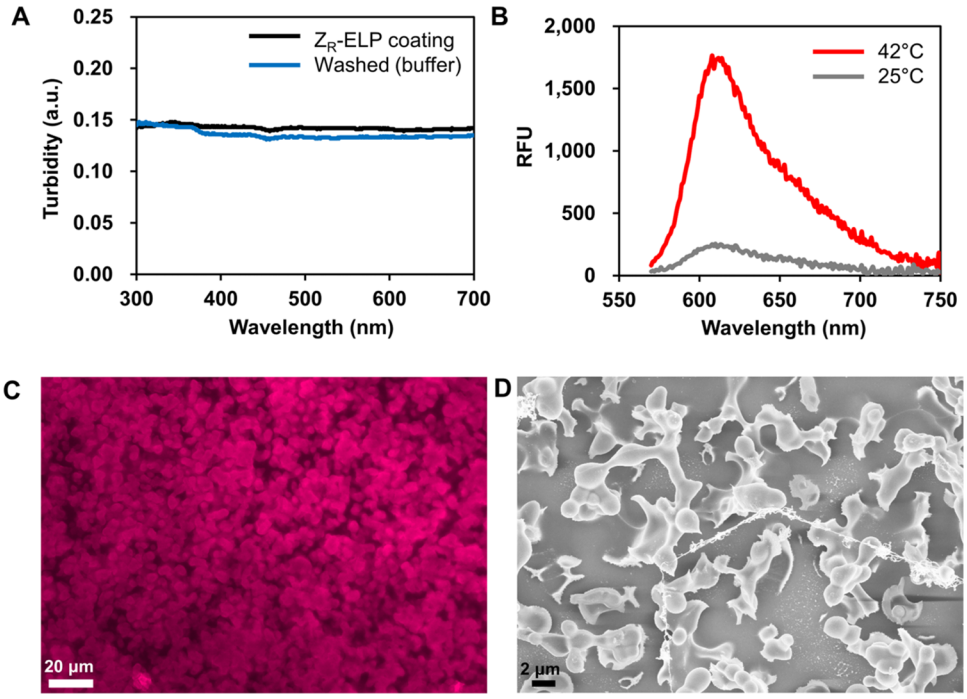

Figure 2. Microstructured protein coating assembly on the glass surfaces. (A) Turbidity profile of Z_R-ELP coating on glass (black) and incubated in buffer for 1 h (blue). (B) Relative fluorescence unit (RFU) of mCherry-Z_E/Z_R-ELP coating prepared at 42 °C (red) and 25 °C (gray). (C) Fluorescence micrograph of the mCherry-Z_E/Z_R-ELP coating prepared at 42 °C. (D) FESEM image of the mCherry-Z_E/Z_R-ELP coating from panel C.

were fused to fluorescent proteins (FPs) or an ELP to construct recombinant fusion proteins, Z_R-ELP and FP-Z_E (Figure 1A,B).[49] While an ELP triggers the self-assembly of protein-rich coacervates through a thermally responsive inverse transition,[49,51,52] the coiled coils Z_E and Z_R mediate strong binding between FP and ELP coacervate. This self-assembly system using FP-Z_E and Z_R-ELP has been exploited to create protein particles in a hydrogel,[53] hollow protein vesicles,[49,54,55] and sheet structures.[56] We expressed and purified a covalently linked Z_R-ELP dimer for protein coating self-assembly (Figures 1A and S1). A disulfide bond at the C-terminal of ELP joins the fusion protein Z_R-ELP to one another, linking the two Z_R domains through an ELP_2 linker (Z_R-ELP_2-Z_R). We hypothesized that this topology is essential for the interconnection of Z_R-ELP coacervates, which can grow into microstructured coating layers.

First, we demonstrated the self-assembly of a fluorescent coating using a red fluorescent protein, mCherry. Fluorescent proteins are robust and easy to characterize and thus ideal for characterizing the self-assembly process. Additionally, many genetically encoded fluorescent biosensors, such as GCaMP, share structural similarities with mCherry, making them excellent model proteins to demonstrate the general applicability of our system. Z_R-ELP coacervates prepared in phosphate-buffered saline (PBS) at 25 °C were first placed on a glass substrate, incubated at 42 °C, and dried. The turbidity of the glass substrate measured at the wavelengths from 300 to 500 nm indicates the formation of a microstructured protein coating, which was stably adhered to the glass surface after an hour of incubation with PBS (Figures 2A and S2). Then, the coating of Z_R-ELP was further incubated with a solution of the recombinant fusion protein mCherry-Z_E and washed. The fluorescence emission at 610 nm (excited at 532 nm) indicates the incorporation of mCherry-Z_E into the protein coating (Figure 2B), which was through the affinity binding interaction between the Z_E and Z_R domains. The fluorescent and confocal micrographs (Figures 2C and S3) showed the interconnection between coacervates, which resulted in the formation of microstructures adhered to the glass. The fluorescence in the images (emission: 610 nm; excitation: 532 nm) further confirmed the attachment of mCherry-Z_E to the microstructured coating. A high-resolution image acquired using a field emission scanning electron microscope (FESEM) also shows the microstructured morphology of the protein coating on glass (Figures 2D and S4A). The morphology of interconnected microspheres at a size of 1.6 ± 0.5 μm was observed according to the image analysis (Figure S4B). This length scale was slightly higher than the hydrodynamic diameter of mCherry-Z_E/Z_R-ELP coacervates measured in an aqueous solution (~0.8 μm, Figure S4C), which would be due to coalescence and growth of the coacervate microspheres on substrates. The result evidence that the microstructures evolved from the partial coalescence between the coacervate microspheres. We hypothesize that while the phase-separated coacervates undergo complete coalescence process in solution phase,[57,58] those deposited on surfaces may experience kinetic hindrance, resulting in the formation of interconnected microstructures. The microstructured protein coating was stably deposited on glass without covalent conjugation or any pretreatment of the glass surfaces.

The formation of microstructures was critically influenced by the temperature. In the coating sample prepared at 25 °C, the formation of microstructures was not observed (Figure S3). Moreover, a remarkably lower fluorescence intensity was measured from the coating (Figure 2B). This could be due to a significant reduction in the surface area of the coating as a result of no microstructure formation. The microstructures are initially formed through the liquid−liquid phase separation of

https://doi.org/10.1021/acsami.4c14249
ACS Appl. Mater. Interfaces 2024, 16, 63284−63294

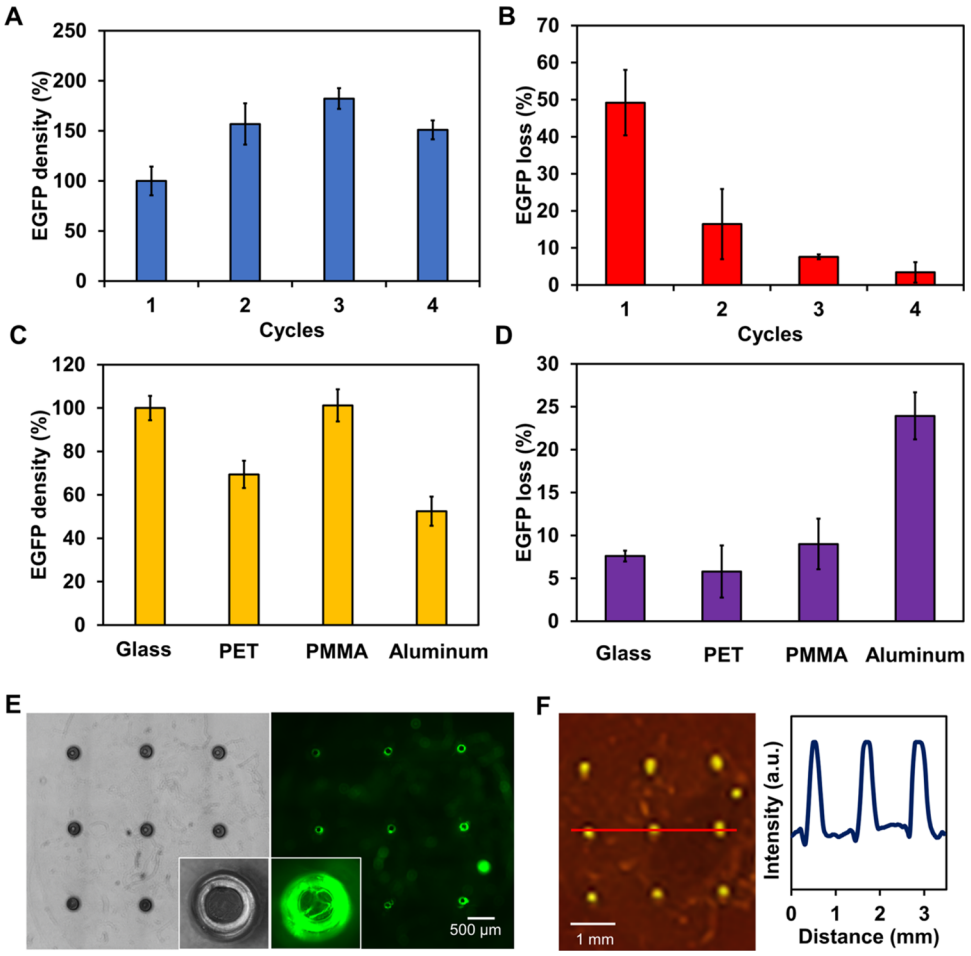

Figure 3. Protein density and stability of self-assembled EGFP-Z_E/Z_R-ELP coatings. (A) Relative protein density of EGFP in the coatings from repeated assembly and deposition cycles. The EGFP densities are normalized to the value from a single cycle. (B) Loss of EGFP from the coatings after 3 h incubation. (C) Relative protein density of EGFP on four distinct substrates: glass, PET, PMMA, and aluminum. The EGFP densities are normalized to the value from glass. (D) Loss of EGFP from the protein coatings after a three h incubation. (E) Micrographs of a protein-coated micropillar array (left: bright field, right: green fluorescence) and the close-up images (insets). (F) Optical image of the protein-coated micropillar array under a transilluminator (left) and the fluorescence intensity profile of a cross-section (indicated by the red line in the left image, right).

Z_R-ELP in solution, which adhere to surfaces and become interconnected (Figure 1). While this process is driven by reversible hydrophobic interactions in the ELP domain, the interconnected microstructures remained stable over time. This is likely caused by structural transformation from α-helix to β-sheet within the coiled coils (Z_R), a change previously observed during heating, drying, or long-term storage of coiled coils in buffer solutions.[59] This transformation is irreversible and helps stabilize the microstructures of the coating (Figure S5). In the absence of β-sheet formation, the microstructures may revert to a soluble protein phase. Therefore, we hypothesize that the conformational transformation is facilitated near the melting temperature of Z_R homodimer (44 °C),[50] serving a critical role in stabilizing the interconnected coacervates.

The Fourier transform infrared (FT-IR) spectrum of the Z_R-ELP coating showed reduced α-helix content and an increased fraction of β-sheet structures, indicating the transition of the secondary structure (Figure S6). The deconvoluted FT-IR spectrum in the amide I region (1600−1700 cm^{-1})[60] exhibits a peak at around 1657 cm^{-1}, with a relative area of 0.917, indicating the presence of 13% α-helix structures. The peaks at 1622 and 1635 cm^{-1} indicate 30% β-sheet structures, with relative areas of 0.962 and 1.185, respectively. In contrast, according to the circular dichroism spectra of soluble Z_R-ELP at 25 °C, the α-helix content is 35.1% and the β-strand is 13.5%.[53] The results evidence the structural transformation of Z_R during the coating assembly.

2.2. Improvement in the Protein Coating Density and Stability for Portable Fluorescence Sensing. As confirmed in Figure 2, fluorescence from the microstructured protein coating can be quantified or imaged by using a spectrofluorometer or microscope. Nonetheless, a portable fluorescent biosensor application would require a simple and low-cost fluorescence reader such as a smartphone camera equipped with a light-emitting diode (LED) and filter. For this to work, the density of protein coatings on a device should be high enough to emit strong quantifiable fluorescence. To increase the protein density, we repeated the steps of coating assembly and deposition (Figure 1C). In addition to mCherry, we used the green fluorescent protein EGFP as a model to also demonstrate the modularity of our system. A droplet of Z_R-ELP solution was placed and dried on a glass surface at 42 °C, followed by incubation with a solution of EGFP-Z_E.[49] This process was repeated for up to four cycles, followed by quantification of fluorescence from EGFP using a portable

https://doi.org/10.1021/acsami.4c14249
ACS Appl. Mater. Interfaces 2024, 16, 63284−63294

LED transilluminator and a smartphone camera (Figures 3A, S7A, and S7B). As a result, the intensity of green fluorescence after three cycles of protein deposition was increased by more than 100% than a single-deposition process. The fluorescence intensity difference between the 3-cycle and 4-cycle protein coatings was not statistically significant (Figure S8). This could be due to surface saturation as the maximum loadable proteins may have been reached after three coating cycles, limiting further EGFP incorporation. Cross-sectional analysis of samples from a single coating cycle revealed uneven fluorescence distribution (Figure S9), which could decrease response intensity and reduce sensitivity in fluorescent biosensor applications. In contrast, the 3-cycle process improved fluorescence homogeneity, a critical factor for enhancing biosensor functionality.

In addition, we observed an increase in the stability of the protein coatings. The repeated deposition of proteins resulted in a reduction in protein loss after long-term incubation of a coating of Z_R-ELP/EGFP-Z_E in buffer (~3 h) (Figure 3B). The coating from a single deposition showed a nearly 50% decrease in the fluorescence from the coating, while it was significantly reduced to below 10% after three or four cycles of repeated protein depositions. We also conducted a negative control experiment to investigate nonspecific physical protein adsorption. Following the protocol for a single cycle without Z_R-ELP, a protein coating was created, and the fluorescence from EGFP was quantified. The results showed that fluorescence intensity was reduced by about seven times (Figure S10), indicating that the EGFP coating is primarily driven by the specific dimerization of Z_E and Z_R, with minimal physical adsorption.

The fluorescence intensity quantified using a smartphone camera was linearly dependent on the concentration of EGFP-Z_E (Figure S11). We correlated the relative fluorescence unit (RFU) and the EGFP-Z_E concentrations using a microplate reader, which was further correlated to the fluorescence intensity quantified from the smartphone images. The result shows a linear relationship between the fluorescence intensity of the coating, the corresponding RFU, and the protein concentration. It verifies the improvement in the density of EGFP incorporated within the coating and the stability of coating attachment. Further in-depth analysis using techniques such as QCM-D could provide precise measurements of the total mass of adsorbed proteins on the surface, which could be correlated with the amount of EGFP incorporated and its overall stability.

2.3. Deposition of Protein Coatings on Four Distinct Substrates. Next, we conducted protein coating assembly on four distinct substrates to demonstrate the versatility of our method. The coating of Z_R-ELP/EGFP-Z_E from three repeated cycles of protein deposition on three different substrates other than glass, including polyethylene terephthalate (PET), poly(methyl methacrylate) (PMMA), and aluminum, showed higher levels of fluorescence intensity, as shown in Figure 3C. The protein coatings on the polymeric substrates (PET and PMMA) had an EGFP density of ~70% and ~100% relative to glass, respectively. Both were as stable as the coating on glass, according to the result from the 3 h stability test (Figure 3D). This finding suggests that similar levels of protein density and stability were achieved using these polymeric substrates, although the coating on aluminum was not as stable as the one on glass. The aromatic and nonaromatic polymers with hydrophobic properties, PET and PMMA, facilitate hydrophobic interactions with Z_R-ELP, while negatively charged glass surfaces enhance the adsorption of Z_R-ELP, which has a positive charge (PI = 11.59 at pH 7.4), through strong electrostatic interactions. In contrast, aluminum may exhibit increased hydrophilicity due to the formation of a thin oxide layer, which could reduce the stability of protein coatings. Overall, the results demonstrate the versatility of our protein coating platform across four distinct glass or polymer substrate materials without covalent conjugation or any pretreatment of the substrates.

In biomedical applications, devices with microarchitectures are often used in combination with biological components like proteins. For example, microneedles are micron-scale medical devices used for transdermal delivery of drugs, vaccines, and other therapeutics.[61−64] To test the feasibility of our coating method on microfabricated surfaces, we conducted protein coating assembly (Z_R-ELP/EGFP-Z_E) on a micropillar array that is widely used for microneedles. After repeated protein coating deposition on the array of micropillars, we imaged them using a fluorescence microscope. The green fluorescence from the micropillars in the micrograph (Figure 3E) indicates the formation of a protein coating on the surface of the micropillars. We were also able to confirm that the green fluorescence could be imaged and quantified using an LED transilluminator and a smartphone camera, followed by imaging analysis (Figure 3F). This indicates that, without functionalization, the formation of dense protein coating was achieved directly from the micropillar array. As demonstrated in Figure 3, our method can be extended to microneedles fabricated using a variety of substrates such as glass and polymers, as surface treatment or functionalization is not necessary. We anticipate our approach will be a good alternative to conventional spray coating methods.[65,66]

2.4. Calcium Sensing for the Detection of Hypercalcemia. Lastly, we demonstrated the application of our protein coating platform for a calcium biosensor using a genetically encoded calcium ion sensor protein GCaMP. The fluorescent biosensor protein is a highly effective Ca^{2+} probe, having a high signal-to-noise ratio with enhanced Ca^{2+} binding affinity (K_D for Ca^{2+} ≈ 235 nM).[67] GCaMP6m, an improved version of GCaMP, was developed by modifying the GCaMP sequence through mutagenesis to enhance its sensitivity and speed.[68] The GCaMP6m protein consists of circularly permuted GFP (cpGFP) and calmodulin (CaM), and the chicken myosin light chain kinase (M13) domains.[69] Upon the binding of Ca^{2+} with CaM and M13, a conformational change occurs, which alters the binding orientation of CaM and M13. This causes a change in the chemical environment surrounding the chromophore in cpGFP, which consequently increases the fluorescence intensity. Because of the critical role of intracellular Ca^{2+} in neuronal signaling, GCaMPs have been used to monitor *in vivo* neuronal activities in the mouse cortex, zebrafish, and insects, after gene transfer and transgenic expression in cells.[68] Extracellular Ca^{2+} also functions as an important messenger[70] and its increased level is associated with diseases like hypercalcemia.[44,71] By assembling a coating of purified GCaMP, we used it to measure the level of Ca^{2+} in biological fluids outside cells.

We designed the recombinant fusion protein GCaMP6m-Z_E for the coating assembly along with Z_R-ELP (Figure S1). After expression and purification from *Escherichia coli*, we confirmed the changes in the absorbance and fluorescence intensities upon Ca^{2+} binding (Figure S12). The absorbance intensity of

https://doi.org/10.1021/acsami.4c14249
ACS Appl. Mater. Interfaces 2024, 16, 63284−63294

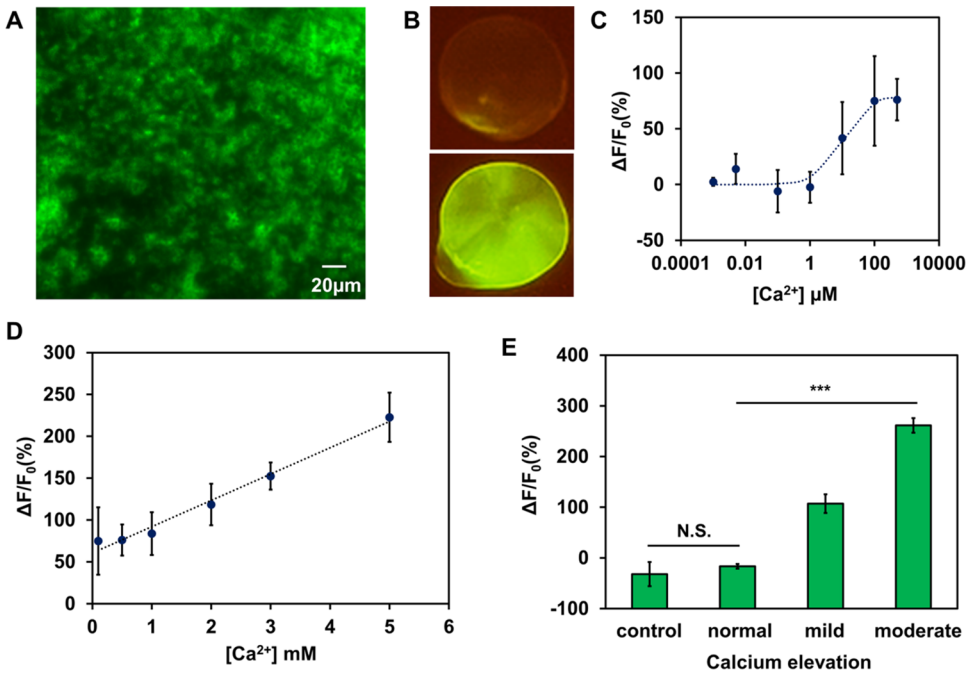

Figure 4. Self-assembled GCaMP6m-Z_E/Z_R-ELP coating. (A) Fluorescent micrograph. (B) Optical images of the coatings under a transilluminator before (top) and after incubation with 5 mM Ca^{2+} (bottom). (C) Ca^{2+}-dependent relative fluorescence intensity ($\Delta F/F_0$) in the range of 1 nM to 500 μM. Experimental data were fitted to a binding model (dotted line) to evaluate $K_{D,app}$. (D) $\Delta F/F_0$ curve in the range of 0.5−5.0 mM. Experimental data were fitted to a linear model (dotted line). (E) $\Delta F/F_0$ response from Tyrode's solution under hypercalcemia-related physiological conditions: control (no calcium), normal (1.3 mM), and mild (1.5 mM) or moderate hypercalcemia (1.8 mM). ***$p \leq 0.005$, and not significant (N.S.). The error bars in (C−E) represent the standard deviation (n = 3).

GCaMP6m-Z_E shows a significant reduction at 496 nm after the addition of a chelating agent, ethylenediaminetetraacetic acid (EDTA) at 100 μM (Figure S12A). It was immediately recovered after the addition of 100 μM calcium chloride. Moreover, the fluorescence intensity of GCaMP6m-Z_E changed in response to the binding of Ca^{2+}, as confirmed by the data in the presence of EDTA or $CaCl_2$ (Figures S12B and C). The results indicate that the sensing ability of GCaMP6m was not affected by the genetic fusion of the Z_E coiled-coil domain. Following the coating assembly procedure described above for Z_R-ELP and EGFP-Z_E, we created a protein coating that included GCaMP6m-Z_E on glass substrates (Figures 4A,B). After three cycles of coating assembly and deposition, the samples were washed and dried. The coating of Z_R-ELP/GCaMP6m-Z_E on glass had a green-emitting fluorescent microstructure, as shown in the micrograph (Figure 4A). To prepare a protein coating in a Ca^{2+}-free state, EDTA (100 μM) was added to a solution of GCaMP6m-Z_E and removed from the coating during the washing step. The protein coating was incubated with aqueous solutions at a range of Ca^{2+} concentrations, and the fluorescence from the coating was imaged using a smartphone camera, followed by image analysis to quantify the intensities. The fluorescence from the Ca^{2+}-free coating was quickly recovered after exposure to Ca^{2+} in water (Figure 4C), and the relative fluorescence intensity ($\Delta F/F_0$) increased up to 76% when the concentrations of Ca^{2+} ranged from 1 nM to 500 μM. The apparent dissociation constant ($K_{D,\ app}$) was ∼11 μM, which is shifted by 2 orders of magnitude from the values for soluble GCaMP6m.[69] The values of $K_{D,\ app}$ in general can be shifted due to the higher target concentration in the microenvironment.[72] In our study, the ELP-based protein coating mimics tissue proteins' microenvironment where Ca^{2+} was far above the K_D of soluble GCaMP6m. Therefore, this shift is most likely due to a higher Ca^{2+} concentration in the microenvironment surrounding the GCaMP probe placed within a protein-rich phase.

The $\Delta F/F_0$ was also plotted against the concentrations of Ca^{2+} in the millimolar level that falls within the calcium levels in the extracellular matrix, from 0.5 to 3.0 mM (Figure 4D).[44,73,74] At this Ca^{2+} concentration level, we observed a drastic change in the fluorescence that was linearly dependent on the concentration of Ca^{2+}. The measured $\Delta F/F_0$ was from 76 to 223% at the Ca^{2+} concentrations of 0.5−5.0 mM, respectively, and an equilibrium binding model did not provide a good fit to the data. This may be due to the complex binding mechanism between GCaMP and Ca^{2+} in this concentration range and more complex binding models such as cooperativity in the ELP domain and Ca^{2+} may need to be considered after additional biophysical characterizations.[75]

The coating of Z_R-ELP/GCaMP6m-Z_E was then used to detect hypercalcemia, which is characterized by elevated Ca^{2+} concentrations in the extracellular fluid. The normal Ca^{2+} concentration is around 1.3 mM, while mild hypercalcemia manifests with Ca^{2+} concentrations around 1.6 mM and moderate hypercalcemia exceeds 1.8 mM.[76] In order to evaluate the sensing ability of our coating platform in the extracellular fluid, we conducted experiments varying Ca^{2+} concentrations in Tyrode's solution that mimics the interstitial fluid. It is a solution with a composition of ions close to the tissue fluid and contains glucose and bovine serum albumin (BSA). The coating incubated with a solution of 1.3 mM Ca^{2+} exhibited $\Delta F/F_0$ of −17 ± 5% (Figure 4E). Conversely, the coating under the mild hypercalcemia condition of 1.5 mM Ca^{2+} showed $\Delta F/F_0$ of 107 ± 18%, while the $\Delta F/F_0$ of the sample under moderate hypercalcemia conditions (1.8 mM) was 261 ± 14%. The $\Delta F/F_0$ values corresponding to mild and

https://doi.org/10.1021/acsami.4c14249
ACS Appl. Mater. Interfaces 2024, 16, 63284−63294

moderate hypercalcemia were significantly higher than those under normal conditions, and the signal difference between mild and moderate hypercalcemia was also significant ($p \leq 0.005$). The reduction of fluorescence under normal or no-calcium conditions could be attributed to the interaction of Ca^{2+} with BSA.[77] In an additional experiment, the relative fluorescence change from tris-buffered saline (TBS) containing Ca^{2+} but no BSA was compared to that of the same buffer that includes Ca^{2+} and 1% BSA (Figure S13). Although a minor decrease in fluorescence was observed with the addition of BSA, statistical analysis indicates that the difference in the fluorescence intensities is not significant.

We conducted additional experiments using mammalian cell culture medium and fetal bovine serum (FBS), which mimic the protein-rich conditions in tissue fluid or blood. Dulbecco's modified Eagle's medium (DMEM) was supplemented with FBS to simulate normal calcemia and hypercalcemia conditions, and the fluorescence intensity changes from protein coatings incubated in the media were quantified. The results showed a 19.5% (±15.9) increase in fluorescence intensity in the normal calcemia region, while increases of 102.3% (±43.5) and 268.5% (±58.5) were observed in mild and moderate hypercalcemia, respectively (Figure S14). Both hypercalcemia conditions showed fluorescence changes statistically different from those under normal calcemia condition. Despite a minor loss in sensitivity, these results validate that our calcium sensor coating could potentially work for blood or tissue fluid samples from patients.

Hypercalcemia is frequently associated with several types of cancers.[71,76] The regulation of calcium homeostasis is interrupted, leading to an increase of the calcium level in the bloodstream above the normal level. During the asymptotic stage, the onset of mild hypercalcemia is associated with cancer development.[76] The fluorescence calcium sensor device demonstrated in this paper showed a sensing ability sufficient to detect mild or moderate hypercalcemia. The current Ca^{2+} sensors for the high concentration range (0.5−3.0 mM) are based on photonic polymers,[38,39] aggregation-induced emission luminogen,[78] functionalized gold nanoparticles,[40,41] and a chemical fluorescence indicator,[44] which require a spectrophotometer or microscope for signal measurement. Genetically modified Ca^{2+} sensors with weaker affinities than GCaMPs operate within this concentration range[79,80] but have only been used to monitor Ca^{2+} dynamics with a fluorescence microscope. In contrast, our detection method operates in a low-resource setting by using a smartphone camera equipped with an LED and light filter, which suggests a potential use for a point-of-care (POC) platform in a clinical setting. The high surface-area-to-volume ratio feature generated by the microstructured coating was critical for the high-density inclusion of fluorescent biosensor proteins like GCaMP, providing enhanced resolution for calcium quantification with these low-resource settings. This feature may also have broader bioengineering applications, particularly where reaction efficiency and mass transfer are critical. Also, our coating fabrication process based on protein solution casting can be extended to the manufacturing of low-cost disposable sensor platforms as demonstrated in portable electrochemical sensors.[81,82] We anticipate that such a platform will facilitate a more accessible and early diagnosis of cancer in combination with the detection of other cancer-related metabolites.

3. CONCLUSIONS

We demonstrated a self-assembly method of protein coatings with microstructural features and programmable functionality by leveraging the modular design of recombinant proteins. The temperature-triggered coacervation through an inverse phase transition followed by noncovalent protein binding of coiled coils resulted in microstructured functional protein coatings. This method is applicable to additional types of substrate materials and modular to program functionality by incorporating globular functional protein domains such as EGFP or GCaMP. We created a calcium biosensor device that quantified the Ca^{2+} level relevant to the detection of hypercalcemia conditions. This modular and versatile protein coating platform is based on a simple, chemical-free, and water-based process under biocompatible conditions. Using the genetically encoded fluorescent biosensor proteins for a variety of targets,[83] we anticipate this platform will provide methods to develop a POC application with rapid and continuous monitoring of disease-associated biomarkers in a low-resource setting.

4. MATERIALS AND METHODS

4.1. Materials. The *E. coli* strain T7 Express *lysY/I*^{q} (BL21 derivative) was purchased from New England Biolabs. The plasmids, pQE60_Z_E/Z_R-ELP, pQE60_mCherry-Z_E, and pQE60_EGFP-Z_E, were kindly provided by J. Champion at the Georgia Institute of Technology. Nickel nitrilotriacetic acid resin (Ni-NTA, HisPur) was purchased from Thermo Scientific. $CaCl_2$ was purchased from the EMD Millipore Corporation. PBS (1×, pH 7.4) containing NaCl (137 mM), KCl (2.7 mM), NaH_2PO_4 (10 mM), KH_2PO_4 (1.8 mM), and TBS (1×, pH 7.4) containing tris base (50 mM) and NaCl (150 mM) were prepared in the lab. Tyrode's solution was made from the lab containing NaCl (135 mM), KCl (2.8 mM), $CaCl_2$ (2 mM), $MgCl_2$ (1 mM), NaH_2PO_4 (400 μM), $NaHCO_3$ (12 mM), glucose (5.5 mM), HEPES (10 mM), and BSA. BSA, FBS, and DMEM were purchased from Thermo Scientific. The substrate materials of glass (0.14 mm thick), PET (0.125 mm thick), and PMMA (1.0 mm thick) were purchased from Globe Scientific, Inc., Calpalmy, and Langaelex, respectively.

4.2. Cloning. The DNA sequences encoding GCaMP6m[69,84] and the Z_E domain[50] were recombined to create a construct encoding GCaMP6m-Z_E. The gene fragment was synthesized, ligated into the *NcoI* and *Bgl*II restriction sites of the pQE60 vector (3.4 kbp), and sequence-verified by GenScript. The resulting plasmid pQE60_GCaMP6m-Z_E was inserted into T7 Express chemically competent cells.

4.3. Protein Expression and Purification. The sequences of recombinant fusion proteins Z_R-ELP, mCherry-Z_E, and EGFP-Z_E are available in Table S1. The recombinant proteins mCherry-Z_E, EGFP-Z_E, and GCaMP6m-Z_E were expressed and purified as previously described.[49,53] Briefly, the cells transformed with the plasmids pQE60_mCherry-Z_E, pQE60_EGFP-Z_E, or pQE60_GCaMP6m-Z_E were grown at 37 °C overnight in 2X yeast extract and tryptone media supplemented with 200 mg/L ampicillin. Overnight protein expression (for 18 h) was induced at the optical density of 0.8 (at 600 nm) by adding 1.0 mM isopropylthio-β-galactoside. After the harvest, cells were lysed with a buffer containing 50 mM Na_2HPO_4, 300 mM NaCl, and 10 mM imidazole and went through a freeze−thaw cycle and sonication. Insoluble parts were removed by centrifugation (10,000 rpm), and the cleared lysate was incubated with Ni-NTA. Then, the recombinant proteins mCherry-Z_E, EGFP-Z_E, or GCaMP6m-Z_E were eluted in a buffer containing 250 mM imidazole after washing. The eluted solution was dialyzed in the 1× TBS. Z_R−ELP was expressed following the same protocol described above and then purified under a denaturing condition using Ni-NTA.[49,53] The expressed complex of His_6Z_E and Z_R-ELP from harvested cells was resuspended in a buffer containing 6 M urea, and

https://doi.org/10.1021/acsami.4c14249
ACS Appl. Mater. Interfaces 2024, 16, 63284−63294

the cleared lysate was incubated with the Ni-NTA resin. After washing, 6 M guanidine hydrochloride was used to elute Z_R-ELP from His_6Z_E bound on the resin. Purified Z_R-ELP was dialyzed into deionized water. The purity and molecular weight of proteins were confirmed by sodium dodecyl sulfate-polyacrylamide gel electrophoresis, followed by time-of-flight mass spectrometry (Waters Xevo G2/XS coupled with nano-ESI). Fluorescence of purified mCherry-Z_E, EGFP-Z_E, and GCaMP6m-Z_E and turbidity of Z_R-ELP coacervates were analyzed by a BioTek SYNERGY H1 microplate reader.

4.4. Protein Coating Assembly. Micropillar arrays were fabricated by ultraviolet light-emitting diode (UV-LED) lithography, which was made using a photosensitive polymer resin.[85] Substrates (glass, PET, PMMA, and aluminum), as well as the microfabricated micropillar arrays, were prepared on a heating block at 42 °C. A 20 μL drop of Z_R-ELP (1.7 mg/mL) was placed and dried on the substrates, followed by incubation with a solution containing 6 μM mCherry-Z_E, EGFP-Z_E, or GCaMP6m-Z_E. These steps were repeated up to three times. The substrates were washed twice with 2× PBS. For a coating of GCaMP6m-Z_E/Z_R-ELP, a solution of GCaMP6m-Z_E was prepared in 100 μM NaCl solution containing 100 μM EDTA. All coatings were dried at room temperature and rinsed with TBS twice for use. For GCaMP6m-Z_E/Z_R-ELP, we stored dried protein coatings at 4 °C overnight before use.

4.5. Microscopy. Protein coatings were imaged by an Olympus IX-73 or Axio Carl Zeiss Observer.Z1 fluorescent microscope with a 40× objective at filter settings of excitation 532 nm/emission 610 nm (mCherry−Z_E) and excitation 488 nm/emission 526 nm (EGFP−Z_E). Confocal microscope images were captured using a Zeiss LSM 510Vis system with a 100× oil immersion objective with laser wavelengths of 543 nm, using a BP 565−615 emission filter. The surface morphology of mCherry-Z_E/Z_R-ELP coating was imaged with a Zeiss Ultra60 FE-SEM. The coating samples were fixed on a glass substrate using 1.0% glutaraldehyde for 1 h, washed twice with deionized water, and subsequently freeze-dried and sputter-coated with gold and imaged at 5 kV.

4.6. Smartphone Imaging and Fluorescence Analysis. The coatings of GCaMP6m-Z_E/Z_R-ELP or EGFP-Z_E/Z_R-ELP were placed under an LED transilluminator (BT Lab Systems) and excited at a wavelength of 470 nm. An iPhone 13 (Apple, Inc.) smartphone with a rear camera (4000 × 3000 pixels) was used to record fluorescence images, which were analyzed by ImageJ. Fluorescence intensity in the green channel of the images was quantified and subtracted by the intensity of background fluorescence. The quantified intensities were normalized by the background intensity and averaged by area. An equally sized area from each image was selected for the analysis. The relative changes in the fluorescence intensity of the protein coating samples in response to Ca^{2+} exposure are calculated using the following equation:

$$\Delta F/F_0 = (F - F_0)/F_0$$

where F_0 represents the initial fluorescence intensity of the protein coating and F denotes the fluorescence intensity after the addition of Ca^{2+}.

4.7. FT-IR Spectroscopy. The FT-IR spectra were recorded on an Agilent Cary 630 FT-IR spectrometer. A 10 μL aliquot of Z_R-ELP coacervate solution in PBS was deposited on a glass substrate at 42 °C. After drying, the Z_R-ELP coating was directly applied to the attenuated total reflection diamond crystal, with the glass substrate serving as a background. Data were analyzed using Agilent MicroLab software, followed by baseline correction and spectrum deconvolution of the amide I peak (1590 and 1710 cm^{-1}) performed using Microsoft Excel.

4.8. Statistical Analysis. Fluorescence recovery responses ($\Delta F/F_0$) were analyzed by one-way analysis of variance (ANOVA) with Tukey's post hoc multiple comparisons or Student's t test for two-group comparison. All statistical analysis was conducted using Microsoft Excel. The p values ≤0.05 were considered statistically significant (*$p \leq 0.05$, **$p \leq 0.01$, ***$p \leq 0.005$, ****$p \leq 0.001$, N.S.; not significant).

■ ASSOCIATED CONTENT

Supporting Information

The Supporting Information is available free of charge at https://pubs.acs.org/doi/10.1021/acsami.4c14249.

Amino acid sequences, SDS-PAGE gels, and mass of recombinant proteins used in this study; bright field, confocal, and FESEM micrographs of protein coatings; size distribution and DLS results of protein coacervates; FT-IR deconvolution result of protein coating; raw data and cross-sectional profiles of fluorescence intensity from protein coatings from different cycles, incubation times, and substrates; calibration curves from smartphone images; UV−vis spectra and fluorescence intensity of soluble GCaMP6m-Z_E; and fluorescence intensity changes under various calcium elevation conditions (PDF)

■ AUTHOR INFORMATION

Corresponding Author

Won Min Park − *Tim Taylor Department of Chemical Engineering, Kansas State University, Manhattan, Kansas 66506, United States;* orcid.org/0000-0002-6076-6353; Email: wmpark@ksu.edu

Authors

Suna Jo − *Tim Taylor Department of Chemical Engineering, Kansas State University, Manhattan, Kansas 66506, United States*

Erin Pearson − *Tim Taylor Department of Chemical Engineering, Kansas State University, Manhattan, Kansas 66506, United States*

Donghoon Yoon − *Division of Hematology Oncology in the Department of Internal Medicine, College of Medicine, University of Arkansas for Medical Science, Little Rock, Arkansas 72205, United States*

Jungkwun Kim − *Department of Electrical Engineering, University of North Texas, Denton, Texas 76207, United States*

Complete contact information is available at: https://pubs.acs.org/10.1021/acsami.4c14249

Author Contributions

S.J. and W.M.P. conceptualized the project with help from D.Y. S.J. and W.M.P. designed proteins, made experimental plans, interpreted the data, and wrote the manuscript with input from all authors. S.J. and E.P. performed protein expression and purification. S.J. and W.M.P. performed coating assembly and characterizations. J.K. designed and fabricated the micropillar arrays. W.M.P. oversaw all aspects of the project. All authors have given approval to the final version of the manuscript.

Funding

This research was funded by grants from the National Science Foundation (2239927) and in part by the Johnson Cancer Research Center at Kansas State University.

Notes

The authors declare no competing financial interest.

■ ACKNOWLEDGMENTS

We acknowledge Prof. Julie Champion (Georgia Institute Technology) for plasmid DNA and Carolina Reyes for technical assistance. We also thank Tej Shrestha at the

Nanotechnology Core in the College of Veterinary Medicine and Prof. Ping Li at the Protein and Biopolymer Analysis Core Lab (Kansas State University) for their assistance in microscope imaging and mass spectrometry.

REFERENCES

(1) Purewal, S. S.; Kaur, A.; Bangar, S. P.; Singh, P.; Singh, H. Protein-Based Films and Coatings: An Innovative Approach. *Coatings* **2024**, *14* (1), 1−24.
(2) Mihalca, V.; Kerezsi, A. D.; Weber, A.; Gruber-traub, C.; Schmucker, J.; Vodnar, D. C.; Dulf, F. V.; Socaci, S. A.; Fărcaş, A.; Mureşan, C. I.; Suharoschi, R.; Pop, O. L. Protein-based Films and Coatings for Food Industry Applications. *Polymers* **2021**, *13* (5), 1−24.
(3) Aigner, T. B.; DeSimone, E.; Scheibel, T. Biomedical Applications of Recombinant Silk-Based Materials. *Adv. Mater.* **2018**, *30* (19), 1−28.
(4) Valo, H. K.; Laaksonen, H.; Peltonen, L. J.; Linder, M. B.; Hirvonen, J. T. Multifunctional Hydrophobin : Toward Nanoparticles. *ACS Nano* **2010**, *4* (3), 1750−1758.
(5) Li, L.; Yang, Y.; Wang, L.; Xu, F.; Li, Y.; He, X. The Effects of Serum Albumin Pre-Adsorption of Nanoparticles on Protein Corona and Membrane Interaction: A Molecular Simulation Study. *J. Mol. Biol.* **2023**, *435* (1), No. 167771.
(6) He, X.; Li, L.; Yang, Y.; Dong, Z.; Wang, L.; Qu, Z.; Xu, F. Tailoring Patchy Nanoparticle Design to Modulate Serum Albumin Adsorption and Membrane Interaction. *Soft Matter* **2021**, *17* (8), 2071−2080.
(7) Liu, Y.; Wu, G.; De Groot, K. Biomimetic Coatings for Bone Tissue Engineering of Critical-Sized Defects. *J. R. Soc., Interface* **2010**, *7* (SUPPL. 5), S631−S647.
(8) Jo, Y. K.; Kim, H. J.; Jeong, Y.; Joo, K. Il.; Cha, H. J. Biomimetic Surface Engineering of Biomaterials by Using Recombinant Mussel Adhesive Proteins. *Adv. Mater. Interfaces* **2018**, *5* (9), 1−13.
(9) Xuan, H.; Tang, X.; Zhu, Y.; Ling, J.; Yang, Y. Freestanding Hyaluronic Acid/Silk-Based Self-Healing Coating toward Tissue Repair with Antibacterial Surface. *ACS Appl. Bio Mater.* **2020**, *3* (3), 1628−1635.
(10) Li, Y.; Li, K.; Wang, X.; Cui, M.; Ge, P.; Zhang, J.; Qiu, F.; Zhong, C.; Zhong, C. Conformable Self-Assembling Amyloid Protein Coatings with Genetically Programmable Functionality. *Sci. Adv.* **2020**, *6* (21), 1−12.
(11) Sahoo, J.; Sharma, R.; Pachauri, V.; Gandhi, S. Biomimetic/Bioderived Nanoengineered Interfaces for Biosensor Applications: A Review. *ACS Appl. Nano Mater.* **2024**, *7* (17), 19854−19875.
(12) Paloni, J. M.; Olsen, B. D. Polymer Domains Control Diffusion in Protein-Polymer Conjugate Biosensors. *ACS Appl. Polym. Mater.* **2020**, *2* (11), 4481−4492.
(13) Grel, H.; Ratajczak, K.; Jakiela, S.; Stobiecka, M. Gated Resonance Energy Transfer (Gret) Controlled by Programmed Death Protein Ligand 1. *Nanomaterials* **2020**, *10* (8), 1−12.
(14) Lefevre, M.; Flammang, P.; Aranko, A. S.; Linder, M. B.; Scheibel, T.; Humenik, M.; Leclercq, M.; Surin, M.; Tafforeau, L.; Wattiez, R.; Leclère, P.; Hennebert, E. Sea Star-Inspired Recombinant Adhesive Proteins Self-Assemble and Adsorb on Surfaces in Aqueous Environments to Form Cytocompatible Coatings. *Acta Biomater.* **2020**, *112*, 62−74.
(15) Qi, H.; Zheng, W.; Zhang, C.; Zhou, X.; Zhang, L. Novel Mussel-Inspired Universal Surface Functionalization Strategy: Protein-Based Coating with Residue-Specific Post-Translational Modification in Vivo. *ACS Appl. Mater. Interfaces* **2019**, *11* (13), 12846−12853.
(16) Qi, H.; Zhang, C.; Guo, H.; Zheng, W.; Yang, J.; Zhou, X.; Zhang, L. Bioinspired Multifunctional Protein Coating for Antifogging, Self-Cleaning, and Antimicrobial Properties. *ACS Appl. Mater. Interfaces* **2019**, *11* (27), 24504−24511.
(17) Tian, J.; Liu, Y.; Miao, S.; Yang, Q.; Hu, X.; Han, Q.; Xue, L.; Yang, P. Amyloid-like Protein Aggregates Combining Antifouling with Antibacterial Activity. *Biomater. Sci.* **2020**, *8* (24), 6903−6911.
(18) Sabaté del Río, J.; Henry, O. Y. F.; Jolly, P.; Ingber, D. E. An Antifouling Coating That Enables Affinity-Based Electrochemical Biosensing in Complex Biological Fluids. *Nat. Nanotechnol.* **2019**, *14* (12), 1143−1149.
(19) Novick, S. J.; Dordick, J. S. Protein-Containing Hydrophobic Coatings and Films. *Biomaterials* **2002**, *23* (2), 441−448.
(20) Xu, X.; Xu, Z. K.; Yang, X. F.; He, Y. H.; Lin, R. Construction and Characterization of a Pure Protein Hydrogel for Drug Delivery Application. *Int. J. Biol. Macromol.* **2017**, *95*, 294−298.
(21) Kimura, Y.; Tabata, Y. Controlled Release of Stromal-Cell-Derived Factor-1 from Gelatin Hydrogels Enhances Angiogenesis. *J. Biomater. Sci., Polym. Ed.* **2010**, *21* (1), 37−51.
(22) Nguyen, P. Q.; Botyanszki, Z.; Tay, P. K. R.; Joshi, N. S. Programmable Biofilm-Based Materials from Engineered Curli Nanofibres. *Nat. Commun.* **2014**, *5*, 1−10.
(23) Song, R.; Wu, X.; Xue, B.; Yang, Y.; Huang, W.; Zeng, G.; Wang, J.; Li, W.; Cao, Y.; Wang, W.; Lu, J.; Dong, H. Principles Governing Catalytic Activity of Self-Assembled Short Peptides. *J. Am. Chem. Soc.* **2019**, *141* (1), 223−231.
(24) Botyanszki, Z.; Tay, P. K. R.; Nguyen, P. Q.; Nussbaumer, M. G.; Joshi, N. S. Engineered Catalytic Biofilms: Site-Specific Enzyme Immobilization onto *E. Coli* Curli Nanofibers. *Biotechnol. Bioeng.* **2015**, *112* (10), 2016−2024.
(25) Nussbaumer, M. G.; Nguyen, P. Q.; Tay, P. K. R.; Naydich, A.; Hysi, E.; Botyanszki, Z.; Joshi, N. S. Bootstrapped Biocatalysis: Biofilm-Derived Materials as Reversibly Functionalizable Multienzyme Surfaces. *ChemCatChem* **2017**, *9* (23), 4328−4333.
(26) Gastaldi, E.; Chalier, P.; Guillemin, A.; Gontard, N. Microstructure of Protein-Coated Paper as Affected by Physico-Chemical Properties of Coating Solutions. *Colloids Surf., A* **2007**, *301* (1−3), 301−310.
(27) Ye, A.; Zhu, Z.; Ji, Z.; He, X.; He, Y.; Fu, X.; Yang, W.; Wang, Y. Electrochemical Active Micro-Protein Coating by Self-Assembling 2D-Microfluidics for Stabilizing Lithium Metal Anode. *Adv. Funct. Mater.* **2024**, *34* (6), 1−13.
(28) Gao, A.; Wu, Q.; Wang, D.; Ha, Y.; Chen, Z.; Yang, P. A Superhydrophobic Surface Templated by Protein Self-Assembly and Emerging Application toward Protein Crystallization. *Adv. Mater.* **2016**, *28* (3), 579−587.
(29) Huang, A.; Qin, G.; Olsen, B. D. Highly Active Biocatalytic Coatings from Protein-Polymer Diblock Copolymers. *ACS Appl. Mater. Interfaces* **2015**, *7* (27), 14660−14669.
(30) Berckman, E. A.; Hartzell, E. J.; Mitkas, A. A.; Sun, Q.; Chen, W. Biological Assembly of Modular Protein Building Blocks as Sensing, Delivery, and Therapeutic Agents. *Annu. Rev. Chem. Biomol. Eng.* **2020**, *11*, 35−62.
(31) Dash, B. C.; Mahor, S.; Carroll, O.; Mathew, A.; Wang, W.; Woodhouse, K. A.; Pandit, A. Tunable Elastin-like Polypeptide Hollow Sphere as a High Payload and Controlled Delivery Gene Depot. *J. Controlled Release* **2011**, *152* (3), 382−392.
(32) Srokowski, E. M.; Woodhouse, K. A. Surface and Adsorption Characteristics of Three Elastin-like Polypeptide Coatings with Varying Sequence Lengths. *J. Mater. Sci.: Mater. Med.* **2013**, *24* (1), 71−84.
(33) Atefyekta, S.; Pihl, M.; Lindsay, C.; Heilshorn, S. C.; Andersson, M. Antibiofilm Elastin-like Polypeptide Coatings: Functionality, Stability, and Selectivity. *Acta Biomater.* **2019**, *83*, 245−256.
(34) Roberts, S.; Dzuricky, M.; Chilkoti, A. Elastin-like Polypeptides as Models of Intrinsically Disordered Proteins. *FEBS Lett.* **2015**, *589* (19), 2477−2486.
(35) Lapenta, F.; Aupič, J.; Strmšek, Ž.; Jerala, R. Coiled Coil Protein Origami: From Modular Design Principles towards Biotechnological Applications. *Chem. Soc. Rev.* **2018**, *47* (10), 3530−3542.

https://doi.org/10.1021/acsami.4c14249
ACS Appl. Mater. Interfaces 2024, 16, 63284−63294

(36) Mandal, R.; Bedewy, M.; Park, W. M. Coiled-Coil Protein Origami Nanostructure Modeling for Improved Characterization and Prediction. *Mol. Syst. Des. Eng.* **2022**, *7*, 725−732.
(37) Park, W. M. Coiled-Coils: The Molecular Zippers That Self-Assemble Protein Nanostructures. *Int. J. Mol. Sci.* **2020**, *21*, 3584.
(38) Moirangthem, M.; Arts, R.; Merkx, M.; Schenning, A. P. H. J. An Optical Sensor Based on a Photonic Polymer Film to Detect Calcium in Serum. *Adv. Funct. Mater.* **2016**, *26* (8), 1154−1160.
(39) Ding, Y.; Ling, J.; Qiao, Y.; Li, Z.; Sun, Z.; Cai, J.; Guo, Y.; Wang, H. A High-Throughput Fluorimetric Microarray with Enhanced Fluorescence and Suppressed "Coffee-Ring" Effects for the Detection of Calcium Ions in Blood. *Sci. Rep.* **2016**, *6* (1), No. 38602.
(40) Kim, S.; Park, J. W.; Kim, D.; Kim, D.; Lee, I.; Jon, S. Bioinspired Colorimetric Detection of Calcium(II) Ions in Serum Using Calsequestrin-Functionalized Gold Nanoparticles. *Angew. Chem., Int. Ed.* **2009**, *121* (23), 4202−4205.
(41) Kim, S.; Kim, J.; Lee, N. H.; Jang, H. H.; Han, M. S. A Colorimetric Selective Sensing Probe for Calcium Ions with Tunable Dynamic Ranges Using Cytidine Triphosphate Stabilized Gold Nanoparticles. *Chem. Commun.* **2011**, *47* (37), 10299−10301.
(42) Golynskiy, M. V.; Gunderson, W. A.; Hendrich, M. P.; Cohen, S. M. Metal Binding Studies and EPR Spectroscopy of the Manganese Transport Regulator MntR. *Biochemistry* **2006**, *45* (51), 15359−15372.
(43) De Acha, N.; Elosúa, C.; Corres, J. M.; Arregui, F. J. Fluorescent Sensors for the Detection of Heavy Metal Ions in Aqueous Media. *Sensors* **2019**, *19* (3), No. 599.
(44) Huang, W.; Wu, T.; Shallan, A.; Kostecki, R.; Rayner, C. K.; Priest, C.; Ebendorff-Heidepriem, H.; Zhao, J. A Multiplexed Microfluidic Platform toward Interrogating Endocrine Function: Simultaneous Sensing of Extracellular Ca^{2+} and Hormone. *ACS Sens.* **2020**, *5* (2), 490−499.
(45) Hove-Madsen, L.; Baudet, S.; Bers, D. M. *Making and Using Calcium-Selective Mini- and Microelectrodes*; Elsevier Inc., 2010; Vol. *99*.
(46) Baudet, S.; Hove-Madsen, L.; Bers, D. M. Chapter 4 How to Make and Use Calcium-Specific Mini- and Microelectrodes. In *Methods in Cell Biology*; Academic Press: New York, 1994; Vol. *40*, 93−113.
(47) Felle, H. Ca^{2+}-Selective Microelectrodes and Their Application to Plant Cells and Tissues. *Plant Physiol.* **1989**, *91* (4), 1239−1242.
(48) Zhang, Y.; Rózsa, M.; Liang, Y.; Bushey, D.; Wei, Z.; Zheng, J.; Reep, D.; Broussard, G. J.; Tsang, A.; Tsegaye, G.; Narayan, S.; Obara, C. J.; Lim, J.-X.; Patel, R.; Zhang, R.; Ahrens, M. B.; Turner, G. C.; Wang, S. S. H.; Korff, W. L.; Schreiter, E. R.; Svoboda, K.; Hasseman, J. P.; Kolb, I.; Looger, L. L. Fast and Sensitive GCaMP Calcium Indicators for Imaging Neural Populations. *Nature* **2023**, *615* (7954), 884−891.
(49) Park, W. M.; Champion, J. A. Thermally Triggered Self-Assembly of Folded Proteins into Vesicles. *J. Am. Chem. Soc.* **2014**, *136* (52), 17906−17909.
(50) Moll, J. R.; Ruvinov, S. B.; Pastan, I.; et al. Designed Heterodimerizing Leucine Zippers with a Ranger of PIs and Stabilities up to 10−15 M. *Protein Sci.* **2001**, *10* (3), 649−655.
(51) Kowalczyk, T.; Hnatuszko-Konka, K.; Gerszberg, A.; Kononowicz, A. K. Elastin-like Polypeptides as a Promising Family of Genetically-Engineered Protein Based Polymers. *World J. Microbiol. Biotechnol.* **2014**, *30* (8), 2141−2152.
(52) Jang, Y.; Hsieh, M.-C.; Dautel, D.; Guo, S.; Grover, M. A.; Champion, J. A. Understanding the Coacervate-to-Vesicle Transition of Globular Fusion Proteins to Engineer Protein Vesicle Size and Membrane Heterogeneity. *Biomacromolecules* **2019**, *20* (9), 3494−3503.
(53) Park, W. M.; Champion, J. A. Two-Step Protein Self-Assembly in the Extracellular Matrix. *Angew. Chem., Int. Ed.* **2013**, *52* (31), 8098−8101.
(54) Dautel, D. R.; Heller, W. T.; Champion, J. A. Protein Vesicles with PH-Responsive Disassembly. *Biomacromolecules* **2022**, *23* (9), 3678−3687.
(55) Dautel, D. R.; Champion, J. A. Protein Vesicles Self-Assembled from Functional Globular Proteins with Different Charge and Size. *Biomacromolecules* **2021**, *22* (1), 116−125.
(56) Dautel, D. R.; Champion, J. A. Self-Assembly of Functional Protein Nanosheets from Thermoresponsive Bolaamphiphiles. *Biomacromolecules* **2022**, *23* (9), 3612−3620.
(57) Urry, D. W.; Trapane, T. L.; Prasad, K. U. Phase-structure Transitions of the Elastin Polypentapeptide−Water System within the Framework of Composition−Temperature Studies. *Biopolymers* **1985**, *24* (12), 2345−2356.
(58) Cirulis, J. T.; Keeley, F. W. Kinetics and Morphology of Self-Assembly of an Elastin-like Polypeptide Based on the Alternating Domain Arrangement of Human Tropoelastin. *Biochemistry* **2010**, *49* (27), 5726−5733.
(59) Roberts, E. K.; Wong, K. M.; Lee, E. J.; Le, M. M.; Patel, D. M.; Paravastu, A. K. Post-Assembly α-Helix to β-Sheet Structural Transformation within SAF-P1/P2a Peptide Nanofibers. *Soft Matter* **2018**, *14* (44), 8986−8996.
(60) Cobb, J. S.; Zai-Rose, V.; Correia, J. J.; Janorkar, A. V. FT-IR Spectroscopic Analysis of the Secondary Structures Present during the Desiccation Induced Aggregation of Elastin-Like Polypeptide on Silica. *ACS Omega* **2020**, *5* (14), 8403−8413.
(61) Kim, Y.-C.; Park, J.-H.; Prausnitz, M. R. Microneedles for Drug and Vaccine Delivery. *Adv. Drug Delivery Rev.* **2012**, *64* (14), 1547−1568.
(62) Chen, J.; Ren, H.; Zhou, P.; Zheng, S.; Du, B.; Liu, X.; Xiao, F. Microneedle-Mediated Drug Delivery for Cutaneous Diseases. *Front. Bioeng. Biotechnol.* **2022**, *10*, No. 1032041.
(63) Dugam, S.; Tade, R.; Dhole, R.; Nangare, S. Emerging Era of Microneedle Array for Pharmaceutical and Biomedical Applications: Recent Advances and Toxicological Perspectives. *Future J. Pharm. Sci.* **2021**, *1*, 1−26.
(64) Liu, F.; Lin, Z.; Jin, Q.; Wu, Q.; Yang, C.; Chen, H. J.; Cao, Z.; Lin, D. A.; Zhou, L.; Hang, T.; He, G.; Xu, Y.; Xia, W.; Tao, J.; Xie, X. Protection of Nanostructures-Integrated Microneedle Biosensor Using Dissolvable Polymer Coating. *ACS Appl. Mater. Interfaces* **2019**, *11* (5), 4809−4819.
(65) Mcgrath, M. G.; Vrdoljak, A.; Mahony, C. O.; Oliveira, J. C.; Moore, A. C.; Crean, A. M. Determination of Parameters for Successful Spray Coating of Silicon Microneedle Arrays. *Int. J. Pharm.* **2011**, *415* (1−2), 140−149.
(66) Chen, Y.; Chen, B. Z.; Wang, Q. L.; Jin, X.; Guo, X. D. Fabrication of Coated Polymer Microneedles for Transdermal Drug Delivery. *J. Controlled Release* **2017**, *265*, 14−21.
(67) Nakai, J.; Ohkura, M.; Imoto, K. A High Signal-to-Noise Ca^{2+} Probe Composed of a Single Green Fluorescent Protein. *Nat. Biotechnol.* **2001**, *19* (2), 137.
(68) Chen, T.-W.; Wardill, T. J.; Sun, Y.; Pulver, S. R.; Renninger, S. L.; Baohan, A.; Schreiter, E. R.; Kerr, R. A.; Orger, M. B.; Jayaraman, V.; et al. Ultrasensitive Fluorescent Proteins for Imaging Neuronal Activity. *Nature* **2013**, *499* (7458), 295−300.
(69) Barnett, L. M.; Hughes, T. E.; Drobizhev, M. Deciphering the Molecular Mechanism Responsible for GCaMP6m's Ca^{2+}-Dependent Change in Fluorescence. *PLoS One* **2017**, *12* (2), No. e0170934.
(70) Hofer, A. M.; Brown, E. M. Extracellular Calcium Sensing and Signalling. *Nat. Rev. Mol. Cell Biol.* **2003**, *4* (7), 530−538.
(71) Walker, M. D.; Shane, E. Hypercalcemia: A Review. *JAMA* **2022**, *328* (16), 1624−1636.
(72) Wang, M.; Kussrow, A. K.; Ocana, M. F.; Chabot, J. R.; Lepsy, C. S.; Bornhop, D. J.; O'Hara, D. M. Physiologically Relevant Binding Affinity Quantification of Monoclonal Antibody PF-00547659 to Mucosal Addressin Cell Adhesion Molecule for in Vitro in Vivo Correlation. *Br. J. Pharmacol.* **2017**, *174* (1), 70−81.
(73) Huang, W.; Wu, T.; Xie, C.; Rayner, C. K.; Priest, C.; Ebendorff-Heidepriem, H.; Zhao, J. Sensing Intra- and Extra-Cellular

Ca2+ in the Islet of Langerhans. *Adv. Funct. Mater.* **2022**, *32* (3), 1−24.
(74) Ishiwari, F.; Hasebe, H.; Matsumura, S.; Hajjaj, F.; Horii-Hayashi, N.; Nishi, M.; Someya, T.; Fukushima, T. Bioinspired Design of a Polymer Gel Sensor for the Realization of Extracellular Ca^{2+} Imaging. *Sci. Rep.* **2016**, *6*, 1−11.
(75) Jarmoskaite, I.; Alsadhan, I.; Vaidyanathan, P. P.; Herschlag, D. How to Measure and Evaluate Binding Affinities. *eLife* **2020**, *9*, 1−34.
(76) Tastanova, A.; Folcher, M.; Müller, M.; Camenisch, G.; Ponti, A.; Horn, T.; Tikhomirova, M. S.; Fussenegger, M. Synthetic Biology-Based Cellular Biomedical Tattoo for Detection of Hypercalcemia Associated with Cancer. *Sci. Transl. Med.* **2018**, *10* (437), No. eaap8562.
(77) Martin, N. H.; Perkins, D. J. The Interaction of Serum Albumins with Calcium. *Biochem. J.* **1950**, *47* (3), 323−326.
(78) Gao, M.; Li, Y.; Chen, X.; Li, S.; Ren, L.; Tang, B. Z. Aggregation-Induced Emission Probe for Light-Up and in Situ Detection of Calcium Ions at High Concentration. *ACS Appl. Mater. Interfaces* **2018**, *10* (17), 14410−14417.
(79) Tang, S.; Wong, H. C.; Wang, Z. M.; Huang, Y.; Zou, J.; Zhuo, Y.; Pennati, A.; Gadda, G.; Delbono, O.; Yang, J. J. Design and Application of a Class of Sensors to Monitor Ca 2+ Dynamics in High Ca^{2+} Concentration Cellular Compartments. *Proc. Natl. Acad. Sci. U.S.A.* **2011**, *108* (39), 16265−16270.
(80) Suzuki, J.; Kanemaru, K.; Ishii, K.; Ohkura, M.; Okubo, Y.; Iino, M. Imaging Intraorganellar Ca^{2+} at Subcellular Resolution Using CEPIA. *Nat. Commun.* **2014**, *5*, 1−13.
(81) Zamani, M.; Robson, J. M.; Fan, A.; Bono, M. S.; Furst, A. L.; Klapperich, C. M. Electrochemical Strategy for Low-Cost Viral Detection. *ACS Cent. Sci.* **2021**, *7* (6), 963−972.
(82) Zamani, M.; Klapperich, C. M.; Furst, A. L. Recent Advances in Gold Electrode Fabrication for Low-Resource Setting Biosensing. *Lab Chip* **2023**, *23* (5), 1410−1419.
(83) Greenwald, E. C.; Mehta, S.; Zhang, J. Genetically Encoded Fluorescent Biosensors Illuminate the Spatiotemporal Regulation of Signaling Networks. *Chem. Rev.* **2018**, *118* (24), 11707−11794.
(84) Molina, R. S.; Qian, Y.; Wu, J.; Shen, Y.; Campbell, R. E.; Drobizhev, M.; Hughes, T. E. Understanding the Fluorescence Change in Red Genetically Encoded Calcium Ion Indicators. *Biophys. J.* **2019**, *116* (10), 1873−1886.
(85) Tan, J. Y.; Li, Y.; Chamani, F.; Tharzeen, A.; Prakash, P.; Natarajan, B.; Sheth, R. A.; Park, W. M.; Kim, A.; Yoon, D.; Kim, J. Experimental Validation of Diffraction Lithography for Fabrication of Solid Microneedles. *Materials* **2022**, *15* (24), 8934.

https://doi.org/10.1021/acsami.4c14249
ACS Appl. Mater. Interfaces 2024, 16, 63284−63294